DMD Fast Forward. Published on September 11, 2008 as doi:10.1124/dmd.108.022624

DMD #22624

Metabolism of 5-isopropyl-6-(5-methyl-1,3,4-oxadiazol-2-yl)-*N*-(2-methyl-1*H*-pyrrolo[2,3-*b*]pyridin-5-yl)pyrrolo[2,1-*f*][1,2,4]triazin-4-amine (BMS-645737): Identification of an Unusual *N*-Acetylglucosamine Conjugate in the Cynomolgus Monkey

Benjamin M. Johnson, Amrita V. Kamath, John E. Leet, Xiaohong Liu, Rajeev S. Bhide, Ravindra W. Tejwani, Yueping Zhang, Ligang Qian, Donna D. Wei, Louis J. Lombardo, and Yue-Zhong Shu

Departments of Pharmaceutical Candidate Optimization (B.M.J., A.V.K., X.L., R.W.T., Y.Z., Y.-Z.S.); New Leads Synthesis and Analysis Technology (J.E.L); and Oncology Chemistry (R.S.B., L.Q., D.D.W., L.J.L.); Bristol-Myers Squibb Pharmaceutical Research Institute, Wallingford, Connecticut

DMD Fast Forward. Published on September 11, 2008 as DOI: 10.1124/dmd.108.022624
This article has not been copyedited and formatted. The final version may differ from this version.

Running title: Metabolism of BMS-645737

Address correspondence to: Dr. Benjamin M. Johnson, Pharmaceutical Candidate Optimization, Bristol-Myers Squibb Company, 5 Research Parkway, Wallingford, CT 06492. email: benjamin.m.johnson@bms.com.

Number of text pages: 37
Number of tables: 3
Number of figures: 4
Number of references: 36
Number of words in the *Abstract*: 191
Number of words in the *Introduction*: 647
Number of words in the *Discussion*: 1084

Nonstandard abbreviations: 1D, one-dimensional; 2D, two-dimensional; BDC, bile-duct cannulated; CID, collision-induced dissociation; DMSO, dimethylsulfoxide; GalcNAc, *N*-acetylgalactosamine; GlcNAc, *N*-acetylglucosamine; GSH, glutathione; HPLC, high-performance liquid chromatography; HSP, hexosamine biosynthetic pathway; KCN, potassium cyanide; LC-MS^n, liquid chromatography-tandem mass spectrometry; *m/z*, mass-to-charge ratio; NADPH, nicotinamide adenine dinucleotide phosphate (reduced form); NMR, nuclear magnetic resonance; NOE, nuclear Overhauser enhancement; OGT, uridine diphospho-*N*-acetylglucosamine:polypeptide β-*N*-acetylglucosaminyltransferase; RTK, receptor tyrosine kinase; SGF, Simulated Gastric Fluid; UDP-GalcNAc, uridine diphospho-*N*-acetylgalactosamine; UDP-GlcNAc, uridine diphospho-*N*-acetylglucosamine; USP, United States Pharmacopeia; VEGF, vascular endothelial growth factor

Abstract

5-Isopropyl-6-(5-methyl-1,3,4-oxadiazol-2-yl)-*N*-(2-methyl-1*H*-pyrrolo[2,3-*b*]pyridin-5-yl)pyrrolo[2,1-*f*][1,2,4] triazin-4-amine (BMS-645737) is a potent and selective VEGF receptor-2 antagonist. In this study, liquid chromatography-tandem mass spectrometry and NMR were used to investigate the biotransformation of BMS-645737 *in vitro* and in the cynomolgus monkey, dog, mouse and rat. Metabolic pathways for BMS-645737 included multi-step processes involving both oxidation and conjugation reactions. For example, the 2-methyl-1*H*-pyrrolo moiety underwent CYP-catalyzed hydroxylation followed by oxidation to a carboxylic acid and then conjugation with taurine. Alternatively, the 5-methyl-1,3,4-oxadiazol-2-yl moiety was metabolized by hydroxylation and then conjugation with sulfate. The pyridin-5-yl group underwent direct glucuronidation in hepatocytes (dog, monkey, human) and conjugation with *N*-acetylglucosamine in the monkey. Conjugation with glutathione and processing along the mercapturic-acid pathway was a minor metabolic pathway *in vivo*, although BMS-645737 did not form conjugates in the presence of glutathione-supplemented liver microsomes. Other minor biotransformation pathways included oxidative dehydrogenation, dihydroxylation, and hydrolytic opening of the oxadiazole ring followed by either deacetylation or hydrolysis of the resulting diacyl hydrazide. Whereas previous studies have demonstrated the formation of *N*-acetylglucosamine conjugates of alcohols, arylamines, and other small molecules, this report describes the biotransformation of a heterocyclic aromatic amine via direct conjugation with *N*-acetylglucosamine.

In recent years, VEGF RTKs have garnered interest as potential therapeutic targets in drug discovery. These receptors are imbedded in the plasma membranes of vascular endothelial cells and are activated by a homologous series of VEGF ligands, most notably a dimeric 45-kDa glycoprotein that is referred to as VEGF or VEGF-A. Binding of VEGF causes these receptors to dimerize and undergo phosphorylation of select tyrosine moieties in the catalytic domain, initiating a cascade that leads to angiogenesis and the growth of blood vessels in the vascular endothelium. In healthy subjects, this process appears to be limited to special circumstances including vasculogenesis during embryonic development (Carmeliet et al., 1996; Ferrara et al., 1996), the growth of bone from cartilage (Kronenberg, 2003), ovarian function (Phillips et al., 1990; Goede et al., 1998) and the healing of damaged tissue (Brown et al., 1992). However, VEGF-mediated angiogenesis is a hallmark of certain hyperproliferative diseases including cancer (Carmeliet, 2005; Jain, 2005) and rheumatoid arthritis (Paleolog and Miotla, 1998). Hence, VEGF receptors offer an attractive target for therapeutic intervention in these diseases, and in particular, VEGF receptor-2, which most closely controls angiogenesis (Kadambi et al., 2001) as well as cancer-cell migration, proliferation and differentiation, stands out as a target of choice in the treatment of cancer. The efficacy of the monoclonal, anti-VEGF antibody bevacizumab (Avastin®, Genentech) in treating metastatic renal-cell (Yang et al., 2003) and rectal carcinomas (Willett et al., 2004) provided a clinical proof-of-concept for sequestering VEGF in cancer therapy. Small-molecule VEGF-receptor antagonists with varying selectivity have also shown promise in the clinic (Bold et al., 2000; Hennequin et al,

2002; Zakarija and Soft, 2005; Traxler, 2003; Wedge et al., 2005; Gingrich et al., 2003; Beebe et al., 2003; Abrams et al., 2003).

BMS-645737 (**1**) is a VEGF receptor-2 antagonist (IC_{50} = 25 nM) belonging to a series of pyrrolotriazine derivatives disclosed previously (Borzilleri et al., 2005; Ruel et al., 2008) (Fig. 1). The biotransformation of compounds with similar structural moieties has been studied previously in the context of other small-molecule therapeutics. For example, the dopamine D_4-selective antagonist L-745,870 was metabolized in the rat, rhesus monkey and human by successive oxidations alpha to azaindole C3, giving 7-azaindole-3-carboxylic acid, and by conjugation to *N*-acetylcysteine, suggesting a bioactivation pathway proceeding via transient imine-methide and glutathionyl intermediates (Zhang et al., 2000). The biotransformation of structurally related indoles, which are used more commonly as building blocks for drug-like molecules, has also been reviewed (Dalvie et al., 2002). Regarding 5-methyl-1,3,4-oxadiazoles, the antidiarrheal agent nufenoxole demonstrated good stability in plasma, urine, and human gastric fluid, and was metabolized in-part by hydroxylation of the 5-methyl moiety in rats and rhesus monkeys but not humans (Cook et al., 1990).

Endogenous steroids such as the bile acid ursodeoxycholic acid (Marschall et al., 1989) and certain metabolites of progesterone (Meng et al., 1996) are eliminated as GlcNAc conjugates in human urine. Conjugation with amino sugars also occurs during the metabolism of certain xenobiotics including selenium (Kobayashi et al., 2002), bisphenol A (Zalko et al., 2003) and nucleotide derivatives such as bohemine (Chmela et al., 2001) and 5-fluorouridine (Weckbecker and Keppler, 1984). The public literature contains one report of arylamine biotransformation in the cynomolgus monkey by this

pathway (Chang et al., 1997), although no GlcNAc conjugates of heterocyclic aromatic amines appear to have been reported previously.

In the present study, the biotransformation of **1** was investigated *in vitro* and in laboratory animals to assist in a broad evaluation of **1** as a clinical-development candidate for the treatment of cancer. In light of the precedents cited above on the biotransformation of azaindole and oxadiazole functional groups, it was hypothesized that multiple oxidative and conjugative pathways would contribute to the metabolism of **1**. This hypothesis was tested by employing a variety of synthetic, biosynthetic and analytical techniques to elucidate the structures of metabolites of **1** and characterize the biotransformation pathways involved in their formation.

Methods

Substances and Enzymes. BMS-645737 (**1**) and compounds **2** {*N*'-acetyl-5-isopropyl-4-[(2-methyl-1*H*-pyrrolo[2,3-*b*]pyridin-5-yl)amino]pyrrolo[2,1-*f*][1,2,4]triazine-6-carbohydrazide}; **3** {5-isopropyl-4-[(2-methyl-1*H*-pyrrolo[2,3-*b*]pyridin-5-yl)amino]pyrrolo[2,1-*f*][1,2,4]triazine-6-carbohydrazide}; **4** {5-isopropyl-4-[(2-methyl-1*H*-pyrrolo[2,3-*b*]pyridin-5-yl)amino]pyrrolo[2,1-*f*][1,2,4]triazine-6-carboxylic acid}; **5** [(5-{5-isopropyl-4-[(2-methyl-1*H*-pyrrolo[2,3-*b*]pyridin-5-yl)amino]pyrrolo[2,1-*f*][1,2,4]triazin-6-yl}-1,3,4-oxadiazol-2-yl)methanol]; and **6** [(5-{[5-isopropyl-6-(5-methyl-1,3,4-oxadiazol-2-yl)pyrrolo[2,1-*f*][1,2,4]triazin-4-yl]amino}-1*H*-pyrrolo[2,3-*b*]pyridin-2-yl)methanol] were synthesized chemically at Bristol-Myers Squibb Co. (Princeton, NJ). All chemical reagents including GSH, KCN, NADPH, UDP-GlcNAc, and UDP-GalcNAc were purchased from Sigma-Aldrich (St. Louis, MO) unless noted otherwise. All solvents (HPLC grade) were purchased from Mallinckrodt Baker (Phillipsburg, NJ). Liver microsomes and S9 (cynomolgus monkey, dog, mouse, rat, human) and expressed human CYP enzymes (Supersomes 1A1, 1A2, 1B1, 2A6, 2B6, 2C8, 2C9, 2C18, 2C19, 2D6, 2E1, 3A4, and 3A5) were obtained from BD Biosciences (San Jose, CA). 1254-Aroclor-induced rat-liver S9 was acquired from Molecular Toxicology, Inc. (Boone, NC).

Preparation of Samples. Compound **1** was incubated together with 1 mM NADPH and liver microsomes (dog, human, monkey, mouse, rat; 1 mg protein/mL) or liver S9 (dog, human, monkey, rat, 1254-Aroclor-induced rat; 5 mg protein/mL), using substrate concentrations of 30 μM and 10 μM, respectively, in 50 mM phosphate buffer (pH 7.4). Incubations (n = 3) of **1** (1 μM) were also carried out in Supersomes expressing

the CYPs 1A1, 1A2, 1B1, 2A6, 2B6, 2C8, 2C9, 2C18, 2C19, 2D6, 2E1, 3A4, and 3A5 (100 pmol CYP protein/mL). Incubations of the diacyl hydrazide **2**, the product of a reaction where the oxadiazole ring of **1** was opened hydrolytically, were also carried out in liver S9 (dog, human, Aroclor-induced rat; 5 mg protein /mL) in order to monitor the formation of **3**. To scale-up the formation of **5** and **6**, 2 mg of **1** (pre-dissolved in 200 µL of DMSO) were mixed with 15 mg of NADPH and 20 mL of 25-mM sodium phosphate buffer (pH 7.4). Depending on the metabolite to be generated, this solution was combined with either 1 mL of CYP 2C19 Supersomes (**5**) or 2 mL of Aroclor-induced rat-liver S9 (**6**). Samples were incubated at 37 °C with constant, gentle shaking and were quenched after 1 h (2 h in scale-up experiments) by adding equal volumes of acetonitrile. Supernatants were analyzed using LC-UV-MS^n.

SGF USP was prepared by combining 2.0 g of sodium chloride, 3.2 g of purified porcine pepsin, 7.0 mL of hydrochloric acid and sufficient water to make 1 L. In an experiment to determine the stability of **1** in SGF over time, approximately 1.2 mg of **1** (free base) and 1.5 mg of **1** (bisulfate salt) were weighed into each of several 10-mL volumetric flasks. To each flask, 1 mL of pre-warmed SGF, USP was added, and the flasks were stored at 37 °C. The pH of these mixtures was approximately 1.2. At each time-point (0, 0.5, 1, 2, 3, 4, 5, 29 h), one flask each of free base and salt was removed from the oven and quenched with 50% aqueous (pH 6.5 phosphate buffer) acetonitrile. The final pH after quenching was approximately 4.0. Aliquots of these solutions were analyzed by HPLC-UV.

The hydroxyl metabolites **5** and **6** were isolated from *in vitro* preparations as follows: supernatants were concentrated to 12 mL under a nitrogen stream to remove

acetonitrile, and the concentrate was diluted with water to 20 mL. This aqueous solution was applied to a Waters Oasis® HLB (12cc, 500mg) pre-packed LP extraction cartridge, washed using a house vacuum with water (50 mL) and then eluted with methanol (50 mL). The methanol eluate was evaporated to dryness and chromatographed using a YMC Pro C18 S-5 (4.6 x 150 mm) column. The mobile phase consisted of 0.1% trifluoroacetic acid in water (Solvent A) and acetonitrile (Solvent B) at a flow rate of 1.2 mL/min with a linear gradient of 10-50% B over 25 minutes; analytes were detected by UV (254 nm). The hydroxyl metabolite **5** (RT = 9.8 min) was obtained from the incubation with expressed CYP2C19, and **6** (RT = 10.6 min) was obtained from the Aroclor-induced rat-liver S9 incubation. Solutions containing both metabolites were collected and lyophilized (< 100 μg each).

Incubations of **1** were carried out in the presence of liver microsomes (human, rat) supplemented with NADPH, GSH and KCN to generate surrogates for chemically reactive metabolites that might have been generated. These samples were prepared by combining 10 μM parent compound, 1 mM NADPH, either 5 mM GSH or 1 mM KCN, and microsomes (1 mg/mL protein) in a 100 mM sodium phosphate buffer solution (pH 7.4) and incubating at 37 °C for 30 min. Reactions were quenched by adding equal volumes of acetonitrile, and the supernatant liquids were recovered for analysis using LC-UV-MS^n.

The biotransformation of **1** was evaluated in suspensions of hepatocytes isolated from the CD-1 mouse, Sprague-Dawley rat, beagle dog, cynomolgus monkey and human. Fresh suspensions of mouse and rat hepatocytes were prepared in-house using a published method (Berry et al, 1991). These hepatocytes were purified by centrifuging a

cell suspension (12.5 mL) with Percoll™ solution (12.5 mL) at 50 × *g* and 4 °C for 5 min. Cells were washed with a suspension buffer and resuspended in an incubation buffer. Cryopreserved human hepatocytes (lot IEM, ECM, HRU), dog hepatocytes (lot LPB), and monkey hepatocytes (lot TGR) were obtained from *In Vitro* Technologies (Baltimore, MD). The gel-entrapped dog, monkey and human hepatocytes were processed in a stepwise manner according to the vendors' instructions, washed with a Krebs-Hensleit suspension buffer (pH 7.4), and resuspended in a Krebs-Hensleit incubation buffer fortified with glucose. Mouse, rat, dog and monkey hepatocytes were from a single donor, whereas the cryopreserved human hepatocytes were pooled from three donors. Cell viability, determined via trypan blue exclusion, was > 85% and > 65% for fresh and cryopreserved hepatocytes, respectively. Compound **1** (30 μM; final organic-solvent content 0.15%) was incubated with hepatocytes (n = 3; density = 0.67 × 10^6 cells/mL) for 2 h at 37 °C, 95% humidity and 5% CO_2. Reactions were quenched using equal volumes of acetonitrile. Supernatants were stored at –20 °C and analyzed using LC-UV-MS^n. Compound **2** was also incubated with hepatocytes (human, mouse) as described above to monitor the formation of **3**. Samples containing hepatocytes (mouse, rat, dog, monkey, human) and either 7-ethoxycoumarin (20 μM) or 7-hydroxycoumarin (20 μM) were prepared as positive controls, and the rate of disappearance of these compounds was monitored to verify the viability of phase-I and phase-II enzymes in these systems.

Studies using animals. All methods were in accordance with the Guide for the Care and Use of Laboratory Animals as adopted by the U.S. National Institutes of Health. Plasma, bile, urine, and GI samples were collected from fasted BDC rats (2 rats/group)

dosed orally with **1** in 0.25% methocel (30 mg/kg). Blood was collected in tubes containing EDTA at 0.25, 0.5, 1, 3, 6, and 9 h after dosing, and plasma was prepared by centrifugation. Bile was collected in 3-h segments over 9 h, and urine (0-9 h) was pooled into a single sample. At the end of the study, the GI tracts and feces were collected and homogenized in 3 volumes of water. Samples were stored at -20 °C until processed further. In support of toxicology studies, an additional high-dose biotransformation study was conducted in non-cannulated, non-fasted male Sprague-Dawley rats (n = 3) that were administered **1** orally via gavage (100 mg/kg). The vehicle was 100% PEG400, and the dosing volume was 10 mL/kg. On the final day of a 10-day toxicokinetics study in female athymic nude mice, blood samples were collected at 1, 5, 8, and 24 h after oral administration of **1** (15, 30, 45, 60 mg/kg/day) in PEG 400:water (1:1). These samples were allowed to clot on ice and then were centrifuged to obtain serum. Plasma and urine samples were also collected following single oral doses of **1** [5 mg/kg in PEG400:0.01N HCl (1:1)] to male cynomolgus monkeys or male beagle dogs (n = 3 for each species). Blood was collected in tubes containing EDTA at 1, 2, 4, 6, 8, and 24 h after dosing, and plasma was obtained by centrifugation. Urine was collected continuously over 24-h intervals. The plasma, urine, and bile samples from each time-point were pooled and treated with an equal volume of acetonitrile (2 volumes for plasma and serum), and all samples were centrifuged for 5 min at 1,000 × *g* to obtain supernatants. These supernatants were stored at 4 °C and analyzed within 24 h using LC-UV-MS^n.

Isolation of Selected Metabolites. Urine was also collected over 0-8 h and 8-24 h intervals following single-dose oral administration of **1** to male cynomolgus monkeys (30, 100, 300 mg/kg) for use in isolating **7** (5-{5-isopropyl-6-(5-methyl-1,3,4-oxadiazol-

2-yl)pyrrolo[1,2-*f*][1,2,4]triazin-4-ylamino}-1*H*-pyrrolo[2,3-*b*]pyridine-2-carboxylic acid), **10** {(*Z*)-3,4,5-trihydroxy-6-(5-{5-isopropyl-6-(5-methyl-1,3,4-oxadiazol-2-yl)pyrrolo[1,2-*f*][1,2,4]triazin-4(3*H*)-ylideneamino}-2-methyl-7*H*-pyrrolo[2,3-*b*]pyridin-7-yl)tetrahydro-2*H*-pyran-2-carboxylic acid} and **11** (*N*-{4,5-dihydroxy-6-(hydroxymethyl)-2-(5-{5-isopropyl-6-(5-methyl-1,3,4-oxadiazol-2-yl)pyrrolo[1,2-*f*][1,2,4]triazin-4-ylamino}-2-methyl-7*H*-pyrrolo[2,3-*b*]pyridin-7-yl)tetrahydro-2*H*-pyran-3-yl}acetamide) in quantities sufficient for NMR analysis. The *N*-linked sugar conjugates **10** and **11** were hydrolytically labile, reverting to **1** and the corresponding sugar moiety slowly at -20 °C or more rapidly under acidic conditions at room temperature; hence, these metabolites were exposed to acid only when necessary and for limited amounts of time. For the isolation, an aliquot from the 8-24 h urine sample was treated with an equal volume of acetonitrile, centrifuged to remove insoluble matter, and concentrated under nitrogen. Metabolites of interest were concentrated further via solid-phase extraction. Typically, a 100-mL aliquot was applied to a Waters Oasis® HLB (35 cc, 6 g) pre-packed LP extraction cartridge, washed (house vacuum) sequentially with water (250 mL) and methanol-water 1:1 (150 mL), and then eluted with methanol (100 mL). The methanol eluate was dried and subjected to preparative HPLC on a Beckman "System Gold" Semipreparative Gradient HPLC, model LC126 (Columbia, MD), using a YMC Pro C18 S-5 (20 × 150 mm) column. The mobile phase consisted of 0.1% trifluoroacetic acid in water (Solvent A) and acetonitrile (Solvent B) at a flow rate of 20 mL/min with a linear gradient of 15-35% B over 25 minutes; analytes were detected by UV (254 nm). Following an injection of extracted material (16 mg/200 µL in DMSO),

DMD Fast Forward. Published on September 11, 2008 as DOI: 10.1124/dmd.108.022624
This article has not been copyedited and formatted. The final version may differ from this version.

the glucuronide **10** (15.6 min), GlcNAc conjugate **11** (16.5 min), and carboxylate **7** (19.8 min) were collected immediately and lyophilized (all < 100 μg each).

Analytical Methods and Instrumentation. An LC-UV-MS method for the analysis of drug-related compound in biologic matrices was developed using an authentic standard of **1**. Chromatographic separations were carried out using a Waters (Milford, MA) Alliance 2695 Separations Module and a Phenomenex (Torrance, CA) CuroSil-PFP (2.0 × 150 mm) column that was maintained at a temperature of 30 °C. The mobile phase consisted of a 95:5 mixture of 0.1% aqueous acetic acid and acetonitrile (Solvent C) and acetonitrile (Solvent D) at a flow rate of 300 μL/min with the following linear gradient conditions: 0% D for 1 min, 0-60% D over 21 min, 60-100% D over 3 min, and 100% D isocratic for 4 min. The eluate from the HPLC column was routed on-line to a Thermo (San Jose, CA) Surveyor photodiode-array detector and then to a Thermo LCQ Deca XP ion trap mass spectrometer. Samples were analyzed using positive-ion electrospray LC-MS^n with data-dependent product-ion scanning. Instrument settings were as follows: *m/z* range = 100 to 900, capillary temperature = 350 °C, nitrogen sheath gas flow rate = 45 (arbitrary units), auxiliary gas = 15, spray voltage = 5.0 kV, capillary voltage = 13 V, tube lens offset = 35 V. Selected samples were also analyzed using a Thermo LTQ-Orbitrap tandem mass spectrometer for chemical-formula determination via accurate-mass measurement. Instrument settings were as follows: MS resolution = 60,000, scan rate = 1/s, *m/z* range = 95 to 1200, capillary temperature = 325 °C, sheath gas = 45, auxiliary gas = 10, source voltage = 4.5 kV, capillary voltage = 30 V, tube lens offset = 85 V. Additionally, **1** exhibited an ultraviolet-absorption maximum of 303 nm. This wavelength was monitored during the analysis of all samples, and the absorbance of

drug-related components at this wavelength was used to make judgments about the relative levels of metabolites therein. It should be noted that this method of semi-quantification was limited by potential differences between the molar absorptivities of **1** and metabolites, and also by the possibility that these components were not resolved chromatographically from endogenous interferences that absorb ultraviolet light.

Isolated metabolites were analyzed using a Varian Inova 600 MHz NMR spectrometer equipped with a 5 mm triple-resonance cold probe. The temperature of the probe was maintained at 25 ºC during all experiments. The metabolites were dissolved in 50 μL of DMSO-d_6 and transferred to 1.7-mm capillary tubes to maximize NMR-detection sensitivity, and small amounts of deuterium chloride were added to enhance peak resolution as needed. The data collected for each metabolite included a ^{1}H-NMR spectrum and a 2D ^{1}H-^{13}C correlation (HSQC) spectrum. NOE experiments (1D or 2D) were performed as needed, and 2D long-range ^{1}H-^{13}C correlation (HMBC) spectra were acquired when sufficient sample was available. Structures of metabolites were elucidated by comparing their ^{1}H and ^{13}C chemical shifts with those of **1** under similar solution conditions.

Results

Positive-ion electrospray MS/MS product ions of **1** were generated via CID and analyzed using a Thermo LTQ-Orbitrap high-resolution mass spectrometer. The monoisotopic mass-to-charge ratios and proposed molecular formulas of these product ions were as follows: *m/z* 306.1105, $C_{15}H_{12}N_7O^{\cdot+}$ (error = 2.3 ppm); *m/z* 347.1371, $[C_{17}H_{14}N_8O + H]^+$ (error = 2.3 ppm); *m/z* 348.1572, $C_{18}H_{18}N_7O^{\cdot+}$ (error = 1.4 ppm). These observations, which were consistent with neutral losses of C_3H_6 (isopropyl group), C_2H_3N (oxadiazole fragment), and C_5H_9N (both isopropyl and oxadiazole fragments) to give the product ions of *m/z* 347, 348, and 306, respectively, were used to assist in elucidating the structures of metabolites of **1**. Compound **1** was incubated with Supersomes containing specific recombinant CYP enzymes, liver microsomes (dog, human, monkey, mouse, rat), liver S9 (dog, human, monkey, rat, Aroclor-induced rat), hepatocytes (dog, human, monkey, mouse, rat), and simulated gastric fluid. It was also administered orally to dogs, monkeys, mice, rats and BDC rats. The biotransformation of **2** was studied using liver S9 (dog, human, Aroclor-induced rat) and hepatocytes (human, mouse). The results of these studies are summarized in Table 1, and proposed biotransformation pathways are illustrated in Fig. 2.

The stability of free-base and bisulfate-salt forms of **1** as suspensions in SGF, USP were examined to simulate *in vivo* conditions after oral dosing and determine the extent of formation of **2** under these conditions. The percentages of **2** that were formed at various time-points are listed in Fig 3. The rate of conversion to **2** was faster for the bisulfate salt than for the free base, most likely because of the higher solubility of the salt form. Compound **2** was not detected following the incubation of **1** in other in vitro

systems, such as liver microsomes or S9. However, **3** was detected following incubations of **2** with liver S9 and hepatocytes, and in S9 this reaction occurred in the presence and absence of NADPH (data not shown).

Although the metabolic turnover of **1** (VEGF receptor-2 IC_{50} = 25 nM) was modest in microsomes from each species, the most abundant metabolites appeared to be the hydroxylation products **5** (IC_{50} = 27 nM) and **6** (IC_{50} > 0.4 μM). The regiochemical arrangement of **5** was confirmed by comparison to an authentic standard and via HSQC NMR (Tables 2 and 3) following its isolation from a large-scale incubation of **1** and CYP2C19 Supersomes. The hydroxylation product **6** was the most abundant metabolite generated by CYP3A4 Supersomes and liver S9 from monkey, dog, human, rat and Aroclor-induced rat. Turnover was comparatively high in Aroclor-induced rat-liver S9, where **7** and a dihydroxylation product were also formed. Considering this high extent of turnover, Aroclor-induced rat-liver S9 was selected as a bioreactor for the formation of **6** in quantities that would allow further characterization. Analysis of this isolated metabolite by HSQC NMR demonstrated attachment of the hydroxyl group to C28, a regiochemical assignment that was also supported by comparing the MS/MS fragmentation patterns of the isolated metabolite **6** with an authentic standard. Although minor metabolites in microsomes included the dehydrogenation product **12**, no adducts were detected following incubations of **1** with microsomes (human, rat) supplemented with either GSH or KCN.

Whereas mouse serum collected 1 h after dosing contained **1** as the major drug-related component, samples collected at 5 h and 8 h also contained high levels of **5** and **9** {(5-{5-isopropyl-4-(2-methyl-1*H*-pyrrolo[2,3-*b*]pyridin-5-ylamino)pyrrolo[1,2-

f][1,2,4]triazin-6-yl}-1,3,4-oxadiazol-2-yl)methyl sulfate}. No drug-related compounds were detected in serum collected 24 h after dosing. The MS^3 product-ion mass spectrum of **9**, following removal of the sulfate moiety via CID, was similar to the MS/MS spectrum of **5.** In contrast, plasma samples that were drawn following single oral doses of **1** to monkeys (5 mg/kg), dogs and rats contained considerably lower levels of **5** than **1**. Plasma samples from the monkey also contained low levels of **10**. Urine collected from dog, monkey and rat all contained **7** as a major metabolite, although **7** was not detected in circulation in any species.

Following oral dosing of **1** to BDC rats, bile that was collected during the post-dose interval of 6-9 h was rich in metabolites compared to samples collected during earlier intervals. Although **6** was not detected in rat bile, **7**-**9** were among the most abundant metabolites in this sample. Additionally, the MS^3 product-ion mass spectrum of **8** {2-(5-{5-isopropyl-6-(5-methyl-1,3,4-oxadiazol-2-yl)pyrrolo[1,2-*f*][1,2,4]triazin-4-ylamino}-1*H*-pyrrolo[2,3-*b*]pyridine-2-carboxamido)ethanesulfonate}, following removal of the putative taurine moiety via CID, was similar to the MS/MS spectrum of **7**. The glutathione conjugate **13**, which was not formed in GSH-supplemented rat-liver microsomes, was a minor component of BDC-rat bile. The fragmentation pattern of **13** included neutral losses of 75 Da (glycine moiety), 129 Da (γ-glutamyl moiety) and 307 Da (GSH). Other components of BDC-rat bile collected at 6-9 h included **1** and **15**-**17**.

Direct conjugation of **1** with certain sugars, resulting in the formation of the *N*-linked conjugates **10** and **11**, contributed to metabolic clearance in hepatocytes from non-rodents. Notably, **11** was the most abundant metabolite in monkey hepatocytes as estimated by LC-UV and was also detected following the incubation of **1** with UDP-

GlcNAc-supplemented monkey liver microsomes. The metabolites **7**, **10**, and **11** were also detected in a pooled urine sample following oral administration of **1** (30, 100, 300 mg/kg) to monkeys. Using a high-resolution mass spectrometer, the monoisotopic mass-to-charge ratios and molecular formulas of these metabolites were determined as follows: **7**, $[M+H]^+$ = 419.1579, $C_{20}H_{18}N_8O_3$ (error = 0.24 ppm); **10**, $[M+H]^+$ = 565.2153, $C_{26}H_{34}N_9O_6$ (1.1 ppm); **11**, $[M+H]^+$ = 592.2629, $C_{28}H_{34}N_9O_6$ (0.51 ppm). During MS/MS with CID, the protonated molecule of **7** lost 18 u (water), and those of **10** and **11** gave characteristic neutral losses of 176 u and 203 u, respectively, corresponding to the masses of glucuronic acid and GlcNAc. Regiochemical assignments for **7**, **10** and **11** were obtained by isolating these metabolites from urine and analyzing them by NMR. Generally, biotransformations produced only small changes in the chemical shifts of ^{13}C and ^{1}H atoms remote from the sites of metabolism, allowing metabolic soft-spots to be identified by comparing the ^{1}H spectra of parent and metabolites. During NMR analysis of both **10** and **11**, an NOE correlation was observed between the anomeric proton of the sugar and H18 of the parent-compound moiety. The glucuronide **10** was further characterized by gHMBC, where both the anomeric proton and H25 of the pyridinyl moiety exhibited 3-bond coupling to C18. Since NMR signals corresponding to the exchangeable 1*H*-pyrrolo proton were not observed during the analysis of either conjugate, and since chemical-shift predictions for C18 were inconsistent with the possibility of a quaternary N19 in proximity, the structures **10** and **11**, with the tautometric forms of the *N*-(2-methyl-1*H*-pyrrolo[2,3-*b*]pyridin-5-yl) moiety shown in Fig. 4, were proposed. When dissolved in DMSO-d_6, several drug-related compounds that were analyzed using NMR exhibited tautomerism on the NMR time-scale, although

the relative amounts of the tautomeric forms varied. For example, two tautomers of **1** and two tautomers of **10** were identified, with the major tautomer of **10** and the minor tautomer of **1** exhibiting the proton H11.

A few minor drug-related components were detected in urine following oral administration of **1** to monkeys at high doses (30, 100, 300 mg/kg) but not a low dose (5 mg/kg). These included **2**, **4**, and a putative mercapturic-acid conjugate **14**. The structure of **14** was proposed based on its molecular weight and fragmentation pattern, which included positive-ion electrospray MS/MS product ions of *m/z* 387 and 421, possibly corresponding to a neutral loss of *N*-acetylcysteine and the product ion RSH^+, respectively. However, this metabolite was not present in a quantity sufficient for isolation and analysis by NMR, precluding a more detailed analysis of its structure.

The arylamine bridge connecting the *N*-(2-methyl-1*H*-pyrrolo[2,3-*b*]pyridin-5-yl and pyrrolo[2,1-*f*][1,2,4] triazin-4-amine moieties was intact in all drug-related compounds identified during biotransformation studies, *i.e.*, no metabolites with free arylamine moieties were detected.

Discussion

Since the conversion of **1** to **2** was observed in simulated gastric fluid but not in other *in vitro* systems, the presence of **2** in urine (monkey, rat) was interpreted to follow from acid-catalyzed hydrolytic ring-opening of the oxadiazole moiety of **1** in the stomachs of these animals following oral dosing. The diacyl hydrazide group of **2** and the acyl hydrazide group of **3** were recognized as potential liabilities in light of certain adverse side effects that have been associated with isoniazid and other hydrazide-containing drugs. The bioactivation of such groups has been shown to involve the formation of nitrogen-centered or alkyl radicals (Goodwin et al., 1996) and entail redox cycling in the presence of peroxidases and redox-active metal ions (Yamamoto and Kawanishi, 1991). None of the hydrazide-containing biotransformation products of **1** were detected in the blood of any animals in the present study, and compounds **2** and **4** were detected in monkey urine following high doses. Although it does not appear to be an issue for **1**, these results do raise the question of whether acid-catalyzed formation of acyl hydrazides from orally delivered xenobiotics containing 1,3,4-oxadiazoles might be a general issue. As mentioned previously, another such compound was found to be stable in a simulated gastric environment (Cook et al., 1990), but the literature contains too few examples for this question to be answered conclusively.

The observation of **5**-**7** and **12** following incubations of **1** in human-liver microsomes, S9 or hepatocytes demonstrated the relevance of multiple pathways for the oxidative biotransformation of **1**. In order to identify the enzymes that catalyzed these reactions, **1** was incubated discretely with 13 of the most important recombinant human CYPs, and supernatants from these incubations were analyzed for the presence of

metabolites. The results suggested that **5** was formed to a large extent by CYPs 2C19, 2C9 and 3A4; and the formation of **6** was catalyzed most effectively by CYPs 3A4, 1B1 and 2C8. Furthermore, the regiochemical arrangements of **6** and **7**, as determined using synthetic standards and NMR, suggest that these metabolites were formed in sequence. A high degree of similarity between the MS/MS product-ion mass spectrum of **7** and the MS^3 product-ion spectrum of **8** indicated that these metabolites were also formed along a common multi-step pathway, and similar reasoning suggested that **5** and **9** were linked sequentially as well. These observations suggested that CYP-catalyzed hydroxylations of C15 and C28 represented "trunk pathways" leading to the formation of downstream metabolites. Such pathways appeared to contribute to metabolic clearance in animals including the BDC rat, where **7**-**9** were abundant components of rat bile. Of these compounds, **7** was anticipated as a metabolite of **1** in humans based on its formation in human hepatocytes and occurrence in the urine of multiple species.

The GSH conjugate **13**, which was detected in rat bile, also might have formed via a multi-step processes involving both oxidative and conjugative components. This pathway is poorly understood because it hasn't been observed *in vitro* and appears to contribute marginally to clearance in the BDC-rat, complicating efforts to isolate a sufficient amount of **13** for analysis by NMR. Previously, the formation of a mercapturic-acid conjugate of a 3-substituted 7-azaindole was proposed to proceed via a transient imine intermediate similar to that in the bioactivation of 3-methyl indoles (Zhang et al., 2000). However, it was difficult to locate the conjugation site of GSH in **13** using MS/MS because the *N*-(2-methyl-1*H*-pyrrolo[2,3-*b*]pyridin-5-yl and pyrrolo[2,1-*f*][1,2,4] triazin-4-amine moieties did not separate readily from each other during CID.

Nevertheless, it is reasonable to assume that **13** and **14** are linked sequentially via the mercapturic-acid pathway, since only one isomer of each metabolite was resolved chromatographically.

The formation of **11** in the monkey was an unexpected outcome that apparently represented a novel biotransformation pathway for heterocyclic amines. This metabolite was not detected in biologic fluids from the dog, mouse or rat, and its formation in the human was not anticipated because it was generated by monkey hepatocytes but not human hepatocytes. Hence, conjugation with GlcNAc appears to be a monkey-specific pathway for the metabolism of **1**. The sample-preparation methods used in this study, which did not entail the acidification of samples immediately after collection, enabled the identification of the *N*-linked sugars **10** and **11**. Such acidification techniques are used commonly in biotransformation studies to stabilize acyl glucuronic-acid conjugates and normalize the pH of bile and urine, which can vary considerably both between and among species. The acidification of samples can assist in the detection of certain metabolites but may have the unintended consequence of hydrolyzing *N*-linked sugars. Such an observation was made previously with respect to the 5-*N*-glucuronic-acid conjugate of clozapine (Breyer-Pfaff and Wachsmuth, 2001). Furthermore, our experience in handling **10** and **11** suggests that both compounds may undergo acid-catalyzed hydrolysis to give **1** and the corresponding free sugar, especially in the presence of a strong acid such as deuterium chloride, which was used selectively in this study during the acquisition of NMR spectra.

The involvement of GlcNAc in drug metabolism is interesting because it is tied to biochemical processes that may fortify certain disease-states including diabetes.

Recently, post-translational modifications of serine and threonine residues by the enzyme OGT have emerged as an important mechanism for the functional regulation of certain proteins, including enzymes involved in metabolism. The HSP, which provides the activated substrate UDP-GlcNAc for these reactions, consumes approximately 4% of cellular glucose and represents an important energetic commitment for the cell. Increased flux through the HSP has been linked to insulin resistance, and the modification of key proteins by *O*-linked GlcNAc may constitute a negative-feedback loop for insulin signaling (Wells and Hart, 2003). Accordingly, the consumption of GlcNAc stores during the biotransformation of xenobiotics might be expected to influence cellular sugar metabolism. Although GlcNAc conjugation of **1** is known only to occur in monkeys, the dynamics of such processes as biochemical and biotransformation pathways compete for a common store of UDP-GlcNAc may be a topic for additional research as xenobiotic acceptors of GlcNAc are identified in humans.

In conclusion, **1** is a potent and selective VEGF receptor-2 antagonist that was considered for development as an angiogenesis suppressor for the treatment of cancer. This compound has 5-methyl-1,3,4-oxadiazol-2-yl and *N*-(2-methyl-1*H*-pyrrolo[2,3-*b*]pyridin-5-yl) moieties that constitute soft-spots for biotransformation in multiple species. In this study, **1** was metabolized by CYP-catalyzed hydroxylation and other oxidative pathways, conjugation with sulfate, taurine, glucuronic acid and GlcNAc (monkey only), and multi-step pathways involving both oxidative and conjugative components. Formation of the GlcNAc conjugate **11** appears to represent a novel biotransformation pathway for heterocyclic amines, possibly with interesting implications for cellular metabolism.

Acknowledgements

We thank Thermo for the use of a LTQ-Orbitrap tandem mass spectrometer, Kevin J. McHale and Thomas Philip for assistance with sample preparation and analysis, Richard A. Westhouse and Ronald G. Lindahl for the collection of animal samples, and Nelly Aranibar, Joseph Fargnoli, Jonathan L. Josephs, David Rodrigues, Punit H. Marathe, Daniel R. Schroeder, and W. Griffith Humphreys for helpful discussions.

References

Abrams TJ, Murray LJ, Pesenti E, Walker Holway V, Colombo T, Lee LB, Cherrington JM, Pryer NK. Preclinical evaluation of the tyrosine kinase inhibitor SU11248 as a single agent and in combination with "standard of care" therapeutic agents for the treatment of breast cancer. *Mol Cancer Ther* 2:1011-1021.

Beebe JS, Jani JP, Knauth E, Goodwin P, Higdon C, Rossi AM, Emerson E, Finkelstein M, Floyd E, Harriman S, Atherton J, Hillerman S, Soderstrom C, Kou K, Gant T, Noe MC, Foster B, Rastinejad F, Marx MA, Schaeffer T, Whalen PM, Roberts WG. Pharmacological characterization of CP-547,632, a novel vascular endothelial growth factor receptor-2 tyrosine kinase inhibitor for cancer therapy. *Cancer Res* 63:7301-7309.

Berry MN, Edwards AM and Barritt GJ. (1991) Isolated hepatocytes preparation, properties and applications, in *Laboratory Techniques in Biochemistry and Molecular Biology* (Berry MN, Edwards AM and Barritt GJ eds) pp 15-58, Elsevier, Amsterdam.

Bold G, Altmann K-H, Frei J, Lang M, Manley PW, Traxler P, Wietfeld B, Brüggen J, Buchdunger E, Cozens R, Ferrari S, Furet P, Hofmann F, Martiny-Baron G, Mestan J, Rösel J, Sills M, Stover D, Acemoglu F, Boss E, Emmenegger R, Lässer L, Masso E, Roth R, Schlachter C, Vetterli W, Wyss D and Wood JM. (2000) New anilinophthalazines as potent and orally well absorbed inhibitors of the VEGF receptor tyrosine kinases useful as antagonists of tumor-driven angiogenesis. *J Med Chem* 43:2310-2323.

Borzilleri RM, Zheng X, Qian L, Ellis C, Cai Z, Wautlet BS, Mortillo S, Jeyaseelan R, Kukral DW, Fura A, Kamath A, Vyas V, Tokarski JS, Barrish JC, Hunt JT, Lombardo LJ, Fargnoli J, Bhide RS (2005) Design, synthesis, and evaluation of orally active 4-(2,4-difluoro-5-(methoxycarbamoyl)phenylamino)pyrrolo[2,1-*f*][1,2,4]triazines as dual vascular endothelial growth factor receptor-2 and fibroblast growth factor receptor-1 inhibitors. *J Med Chem* 48:3991-4008.

Breyer-Pfaff U and Wachsmuth H (2001) Tertiary N-glucuronides of clozapine and its metabolites desmethylclozapine in patient urine. *Drug Metab Dispos* 29:1343-1348.

Brown LF, Yeo KT, Berse B, Yeo TK, Senger DR, Dvorak HF and van de Water L (1992) Expression of vascular permeability factor (vascular endothelial growth factor) by epidermal keratinocytes during wound healing. *J Exp Med* 176:1375-1379.

Carmeliet P, Ferreira V, Breier G, Pollefeyt S, Kieckens L, Gertsenstein M, Fahrig M, Vandenhoeck A, Harpal K, Eberhardt C, Declercq C, Pawling J, Moons L, Collen D, Risau W and Nagy A (1996) Abnormal blood vessel development and lethality in embryos lacking a single VEGF allele. *Nature* 380:435-439.

Chang M, Sood VK, Kloosterman DA, Hauer MJ, Fagerness PE, Sanders PE and Vrbanac JJ (1997) Identification of the metabolites of the HIV-1 reverse transcriptase inhibitor delavirdine in monkeys. *Drug Metab Dispos* 25:814-827.

Chmela Z, Veselý J, Lemr K, Rypka M, Hanuš J, Havlíček L, Kryštof V, Michnová L, Fuksová K and Lukeš J (2001) In vivo metabolism of 2,6,9-trisubstituted purine-derived cyclin-dependent kinase inhibitor bohemine in mice: glucosidation as the principal metabolic route. *Drug Metab Dispos* 29:326-334.

Cook CS, Campion JG, Hribar JD and Karim A (1990) Metabolism and pharmacokinetics of nufenoxole in animals and humans: an example of stereospecific hydroxylation of an isoquinuclidine ring. *Xenobiotica* 20:1065-1080.

Dalvie DK, Kalgutkar AS, Khojasteh-Bakht SC, Obach RS and O'Donnell JP (2002) Biotransformation reactions of five-membered aromatic heterocyclic rings. *Chem Res Toxicol* 15:269-299.

Ferrara N, Carver-Moore K, Chen H, Dowd M, Lu L, O'Shea KS, Powell-Braxton L, Hillan KJ and Moore MW (1996) Heterozygous embryonic lethality induced by targeted inactivation of the VEGF gene. *Nature* 380:439-442.

Gingrich DE, Reddy DR, Iqbal MA, Singh J, Aimone LD, Angeles TS, Albom M, Yang S, Ator MA, Meyer SL, Robinson C, Ruggeri BA, Dionne CA, Vaught JL, Mallamo JP, Hudkins RL. A new class of potent vascular growth factor receptor tyrosine kinase inhibitors: structure-activity relationships for a series of 9-alkoxymethyl-12-(3-hydroxypropyl)-indeno[2,1-*a*]pyrrolo[3,4-*c*]carbazole-5-ones and the identification of

CEP-5214 and its dimethylglycine ester prodrug clinical candidate CEP-7055. *J Med Chem* 46:5375-5388.

Goede V, Schmidt T, Kimmina S, Kozian D and Augustin HG (1998) Analysis of blood vessel maturation processes during cyclic ovarian angiogenesis. *Lab Invest* 78:1835-1894.

Goodwin DC, Aust SD and Grover TA (1996) Free radicals produced during the oxidation of hydrazines by hypochlorous acid. *Chem Res Toxicol* 9:1333-1339.

Hennequin LF, Stokes ES, Thomas AP, Johnstone C, Ple PA, Ogilvie DJ, Dukes M, Wedge SR, Kendrew J and Curwen JO (2002) Novel 4-anilinoquinazolines with C-7 basic side chains: design and structure activity relationship of a series of potent, orally active, VEFG receptor tyrosine kinase inhibitors. *J Med Chem* 45:1300-1312.

Jain RK (2005) Normalization of tumor vasculature: an emerging concept in antiangiogenic therapy. *Science* 307:58-62.

Kadambi A, Mouta Carreira C, Yun CO, Padera TP, Dolmans DE, Carmeliet P, Fukumura D and Jain RK. (2001) Vascular endothelial growth factor (VEGF)-C differentially affects tumor vascular function and leukocyte recruitment: role of VEGF-receptor 2 and host VEGF-A. *Cancer Res* 61:2404-2408

Kobayashi Y, Ogra Y, Ishiwata K, Takayama H, Aimi N and Suzuki KT (2002) Selenosugars are key and urinary metabolites for selenium excretion within the required to low-toxic range. *Proc Nat Acad Sci* 99:15932-15936.

Kronenberg HM (2003) Developmental regulation of the growth plate. *Nature* 423:332-336.

Marschall H-U, Egestad B, Matern H, Matern S and Sjövall J (1989) *N*-acetylglucosaminides: a new type of bile acid conjugate in man. *J Biol Chem* 264:12989-12993.

Meng LJ, Griffiths WJ and Sjövall J (1996) The identification of novel steroid *N*-acetylglucosaminides in the urine of pregnant women. *J Steroid Biochem Molec Biol* 58:585-598.

Paleolog EM and Miotla JM (1998) Angiogenesis in arthritis: role in disease pathogenesis and as a potential therapeutic target. *Angiogenesis* 2:295-307.

Phillips HS, Hains J, Leung DW and Ferrara N (1990) Vascular endothelial growth factor is expressed in rat corpus luteum. *Endocrinology* 127:965-967.

Ruel R, Thibeault C, L'Heureux A, Martel A, Cai Z-W, Wei D, Qian L, Barrish JC, Mathur A, D'Arienzo C, Hunt JT, Kamath A, Marathe P, Zhang Y, Derbin G, Wautlet B,

Mortillo S, Jeyaseelan R, Henley B, Tejwani R, Bhide R, Trainor GL, Fargnoli J, Lombardo LJ (2008) Discovery and Preclinical Studies of 5-Isopropyl-6-(5-methyl-1,3,4-oxadiazol-2-yl)-*N*-(2-methyl-1*H*-pyrrolo[2,3-*b*]pyridin-5-yl)pyrrolo[2,1-*f*][1,2,4] triazin-4-amine (BMS-645737), an *In Vivo* Active Potent VEGFR-2 Inhibitor. *Bioorg Med Chem Lett* 18:2985-2989.

Traxler P (2003) Tyrosine kinases as targets in cancer therapy - successes and failures. *Exp Opin Ther Targets* 7:215.

Weckbecker G and Keppler DO (1984) Substrate properties of 5-fluorouridine diphospho sugars detected in hepatoma cells. *Biochem Pharmacol* 33:2291-2298.

Wedge SR, Kendrew J, Hennequin LF, Valentine PJ, Barry ST, Brave SR, Smith NR, James NH, Dukes M, Curwen JO, Chester R, Jackson JA, Boffey SJ, Kilburn LL, Barnett S, Richmond GHP, Wadsworth PF, Walker M, Bigley AL, Taylor ST, Cooper L, Beck S, Jurgensmeier JM, Ogilvie DJ. AZD2171: A highly potent, orally available, vascular growth factor receptor-2 tyrosine kinase inhibitor for the treatment of cancer. *Cancer Res* 65:4389-4400.

Wells L and Hart GW (2003) O-GlcNAc turns twenty: functional implications for post-translational modification of nuclear and cytosolic proteins with a sugar. *FEBS Lett* 546:154-158.

Willett CG, Boucher Y, di Tomaso E, Duda DG, Munn LL, Tong RT, Chung DC, Sahani DV, Kalva SP, Kozin SV, Mino M, Cohen KS, Scadden DT, Hartford AC, Fischman AJ, Clark JW, Ryan DP, Zhu AX, Blaszkowsky LS, Chen HX, Shellito PC, Lauwers GY and Jain RK (2004) Direct evidence that the VEGF-specific antibody bevacizumab has antivascular effects in human rectal cancer. *Nature Med* 10:145-147.

Yamamoto K and Kawanishi S (1991) Free radical production and site specific DNA damage induced by hydralazine in the presence of metal ions or peroxidase/hydrogen peroxide. *Biochem Pharmacol* 41:905-914.

Yang JC, Haworth L, Sherry RM, Hwu P, Schwartzentruber DJ, Topalian SL, Steinberg SM, Chen HX and Rosenberg SA (2003) A randomized trial of bevacizumab, an anti-vascular endothelial growth factor antibody, for metastatic renal cancer. *N Engl J Med* 349:427-434.

Zakarija A and Soft G (2005) Update on angiogenesis inhibitors. *Curr Opin Oncol* 17:578-583.

Zalko D, Soto AM, Dolo L, Dorio C, Rathahao E, Debrauwer L, Faure R and Cravedi J-P (2003) Biotransformations of bisphenol A in a mammalian model: answers and new questions raised by low-dose metabolic fate studies in pregnant CD1 mice. *Environ Health Perspect* 111:309-319.

Zhang KE, Kari PH, Davis MR, Doss G, Baillie TA and Vyas KP (2000) Metabolism of a dopamine D_4-selective antagonist in rat, monkey, and humans: formation of a novel mercapturic acid adduct. *Drug Metab Dispos* 28:633-642.

Legends

Fig. 1. *Structure of BMS-645737 (**1**) with atoms numbered.*

Atom numbers are for illustrative purposes and do not conform to IUPAC nomenclature.

Fig. 2. *Pathways proposed for the biotransformation of BMS-645737 (**1**).*

The diacyl hydrazide **2** was formed in SGF, and **3** was formed independently of NADPH in liver S9. The hydroxylation products **5** and **6** were formed by certain CYPs and then metabolized further as shown. Of the *N*-linked sugars, **10** was a major metabolite in non-rodent hepatocytes, and **11** was detected in monkey microsomes, hepatocytes and urine. The *S*-linked conjugates **13** and **14** were minor metabolites *in vivo* based on LC-UV analysis.

Fig. 3. *Stability of BMS-645737 (**1**) in Simulated Gastric Fluid, USP. The percentage of the diacyl hydrazide **2**, formed via hydrolytic opening of the 5-methyl-1,3,4-oxadiazol-2-yl ring, was measured via LC-UV following incubations of free-base and bisulfate-salt forms of **1** in SGF at 37 °C.*

Fig. 4. *NOE correlations observed during NMR analysis of the glucuronic-acid conjugate (**10**) and GlcNAc conjugate (**11**) of BMS-645737 (**1**).*

DMD Fast Forward. Published on September 11, 2008 as DOI: 10.1124/dmd.108.022624
This article has not been copyedited and formatted. The final version may differ from this version.

TABLE 1

Mass spectrometric data and proposed biotransformation pathways leading to selected metabolites of BMS-645737 in vitro *and in animals*

A normalized collision energy of 40% was used to generate the product ions listed. In certain cases, metabolic pathways were proposed based on both MS and NMR data. Abbreviations: D, dog; H, human; M, cynomolgus monkey; Ms, mouse; R, rat; AIR, Aroclor-induced rat; NA, not applicable.

Compound	Precursor Ion $[M+H]^+$	Product Ions *m/z*	Proposed Biotransformation Pathway	Detected In
1	389	306, 347, 348	NA	All samples treated with **1**
2[a]	407	333, 351, 352, 365, 389	Hydrolysis of oxadiazole to diacyl hydrazide	Simulated gastric fluid, urine (M, R)
3[b]	365	291, 306, 323, 333, 348, 351	Deacetylation of **2**	Incubations of **2** in liver S9 (D, H, AIR) and hepatocytes (H, M)
4	351	265, 291, 309, 333	Hydrolysis of **2** and/or **3** to carboxylic acid	Urine (M)
5	405	290, 332, 348, 363, 375	Hydroxylation of C15	Liver microsomes (D, H, M, Ms, R), CYPs 2C9, 2C19 and 3A4, liver S9 (D, H, M, R), hepatocytes (D, H, M, R), serum (Ms), plasma (D, M, R)
6	405	290, 332, 345, 363, 375, 387	Hydroxylation of C28	Liver microsomes (D, H, M, Ms, R), CYPs 1A2, 1B1, 2C8, 2C9, 2C19, 2D6, 3A4, liver S9 (D, H, M, R, AIR)
7	419	333, 377, 401	Oxidation of **6** to carboxylate	Liver S9 (AIR), hepatocytes (D, H, M, R), bile (BDC R), urine (D, M, R)
8	526	401, 419	Conjugation of **7** with taurine	Bile (BDC R), urine (M)
9	485	387, 405	Sulfation of **5**	Serum (Ms), urine (M)
10	565	389	Conjugation of N19 with glucuronic acid	Hepatocytes (D, H, M), plasma and urine (M)
11[c]	592	389	Conjugation of N19 with GlcNAc	UDP-GlcNAc-supplemented liver microsomes, hepatocytes and urine (M only)
12	387	304, 345, 346	Dehydrogenation	Liver microsomes (H, M, Ms, R), and S9 (H, M)
13	694	387, 421, 565, 619, 676	Conjugation with glutathione	Bile (BDC R)
14	550	333, 389, 419, 421, 508	Dihydrolysis of **13** and acetylation to a mercapturic acid	Urine (M)
15, 16[d]	581	405	Hydroxylation and glucuronidation	Hepatocytes (M), Bile (BDC R)
17	435	362, 378, 393, 405, 417	Hydroxylation of **7**	Bile (BDC R)

[a] No enzymatic pathways for the formation of **2** were identified.

[b] Compound **3** was not detected as a metabolite of **1** in any systems. However, **2** was deacetylated to give **3** independently of NADPH in liver S9.

[c] The negative-ion electrospray product-ion mass spectrum of **11** exhibited a single intense peak of *m/z* 387.

[d] Although the metabolites **15** and **16** were differentiated based on HPLC retention time and MS^3 spectra, their regiochemical arrangements were not determined.

Table 2

Chemical Shifts and Coupling Constants (J) of BMS-645737[a] that were observed using NMR

The ^{1}H and ^{13}C chemical shifts listed below were measured with respect to the solvent-lock frequency of $(CH_3)_4Si$ at 0.0 ppm. The ^{15}N chemical shifts were referenced by the solvent-lock frequencies of $^{15}NH_4{}^{15}NO_3$ at 20.7 and 376.3 ppm. The ^{13}C and ^{15}N chemical shifts were extracted from the indirect dimension of 2D NMR experiments. Atom numbers do not conform to IUPAC nomenclature.

Atom Number	^{1}H	^{13}C	^{15}N
1	-	-	-
2	-	161.7/NA[b]	-
3	-	-	NA
4	-	-	300.4/300.3
5	-	163.9/163.2	-
6	-	107.9/NA	-
7	8.16/7.80 (s, 1H)	120.9/121.2	-
8	-	-	206.2/204.9
9	-	-	257.6/242.0
10	7.81 (s, 1H)/7.33 (d, *J*=4)	148.5/139.8	-
11	/10.25 (d, *J*=4, 1H)	-	206.2/126.6
12	-	155.4/NA	-
13	-	112.7/NA	-
14	-	124.5/129.2	-
15	2.54/2.51 (s, 3H)	11.0/11.0	-
16	-	-	105.7/NA
17	-	127.1/NA	-
18	8.11/7.66 (d, *J*=2, 1H)	140.2/135.2	-
19	-	-	NA
20	-	147.1/146.7	-
21	11.47/11.29 (s, 1H)	-	142.7/142.5
22	-	138.2/137.7	-
23	6.13/6.04 (s, 1H)	98.3/98.0	-
24	-	121.0/121.6	-
25	7.84/7.26 (d, *J*=2, 1H)	125.2/118.7	-
26	3.94/4.42 (m, 1H)	26.5/25.1	-
27,29	1.41/1.36 (d, *J*=7)	22.6/21.6	-
28	2.37/2.35 (s, 3H)	14.2/14.2	-

[a] BMS-645737 was observed as a mixture of two tautomers in DMSO-d_6. The first chemical shift in each cell corresponds to the major tautomer and the second to the minor tautomer.

[b] NA: not applicable because no correlation was observed in 2D experiments.

DMD Fast Forward. Published on September 11, 2008 as DOI: 10.1124/dmd.108.022624
This article has not been copyedited and formatted. The final version may differ from this version.

Table 3

A summary of NMR observations that were used to elucidate the structures of isolated metabolites of BMS-645737

Compound	Key NMR Observations and Conclusions
5	The location of the hydroxyl group at C15 was assigned based on the and the presence of a new 4.68/54.0 ppm cross-peak in the ^{1}H-^{13}C HSQC spectrum, signifying a CH_2OH group, and the absence of the H15/C15 (2.54/11.0 ppm) cross-peak that was observed in the NMR spectrum of **1**
6	The location of the hydroxyl group at C28 were inferred from the presence of a new 4.6/57.0 ppm cross-peak in the ^{1}H-^{13}C HSQC spectrum, signifying a CH_2OH group, and the absence of the H28/C28 (2.37/2.35 ppm; 14.2/14.2 ppm) cross-peak
7	The location of the carboxylate group at C28 was inferred from the absence of the H28/C28 (2.37/2.35 ppm; 14.2/14.2 ppm) cross-peak and the absence of other cross-peaks in the ^{1}H-^{13}C HSQC spectrum
10	Only one tautomer was observed. The anomeric proton exhibited a chemical shift of 6.3 ppm/90 ppm. Location of the glucuronic acid moiety was inferred from an NOE correlation between the anomeric proton and H18
11	The anomeric $^{1}H/^{13}C$ of the major and minor tautomers exhibited chemical shifts of 6.0 ppm/91 ppm and 6.1 ppm/90 ppm, respectively. Location of the GlcNAc moiety was inferred from correlations of C18 to both the anomeric proton and H25 (major tautomer) in the ^{1}H-^{13}C gHMBC spectrum

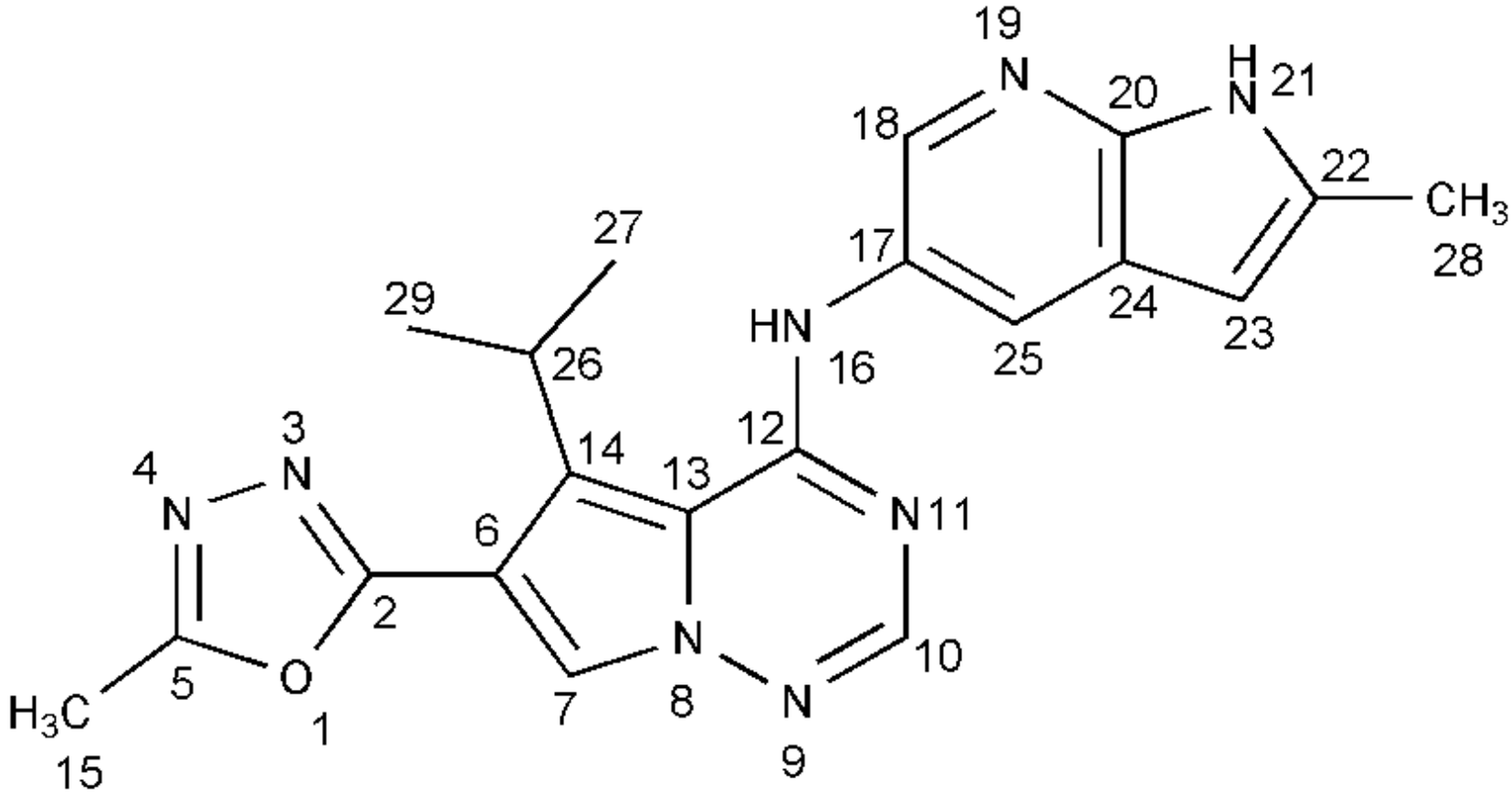
19
N
H
N
21
20
18
22
CH3
28
17
27
29
24
23
HN
16
25
26
12
3
14
13
4
N
N
N11
6
2
N
10
5
O
7
8
N
H3C
1
9
15

Fig 1

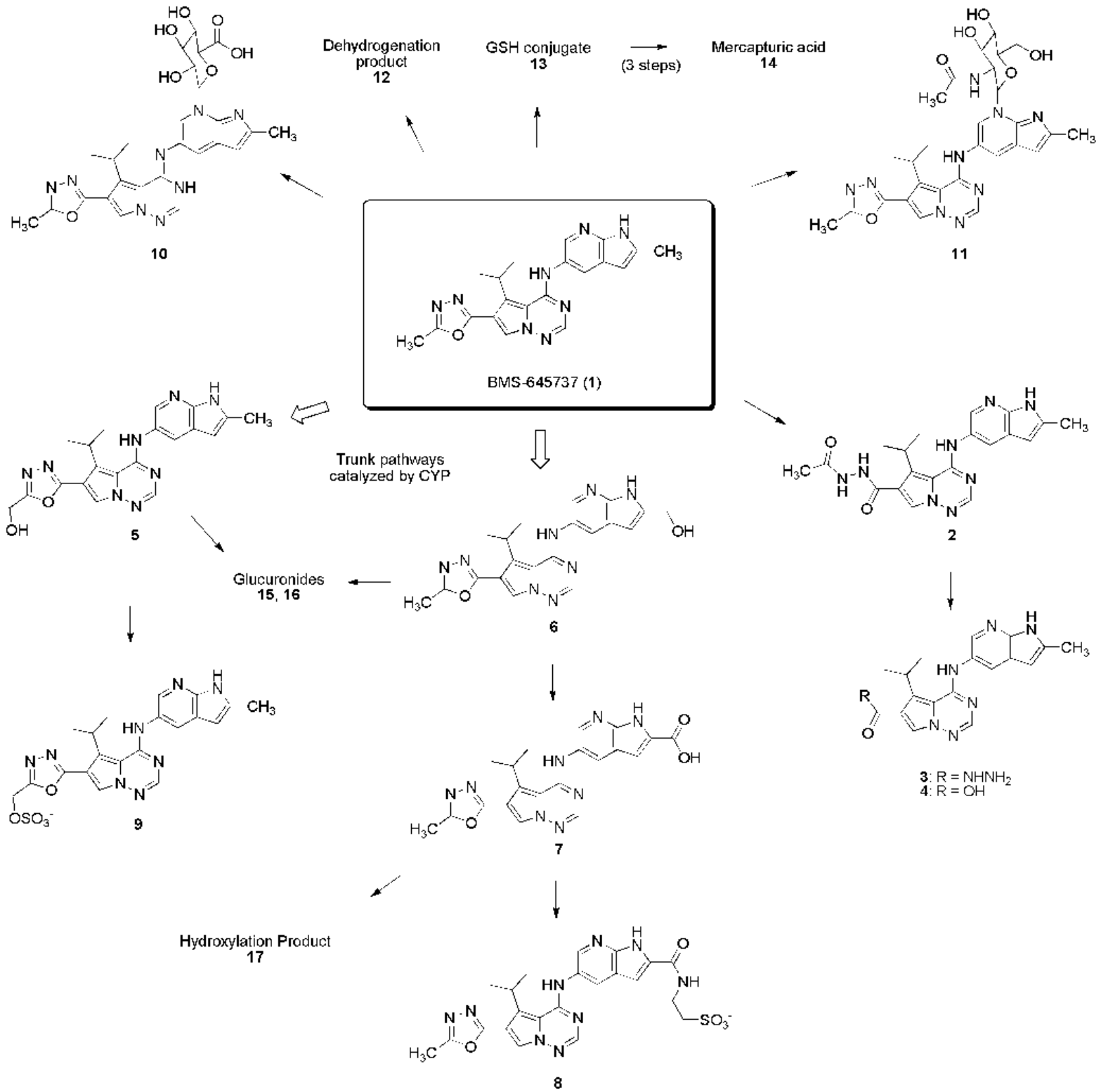
Dehydrogenation product
12
GSH conjugate
13
(3 steps)
Mercapturic acid
14
10
11
BMS-645737 (1)
Trunk pathways catalyzed by CYP
5
2
Glucuronides
15, 16
6
3: R = NHNH2
4: R = OH
9
7
Hydroxylation Product
17
8

Fig 2

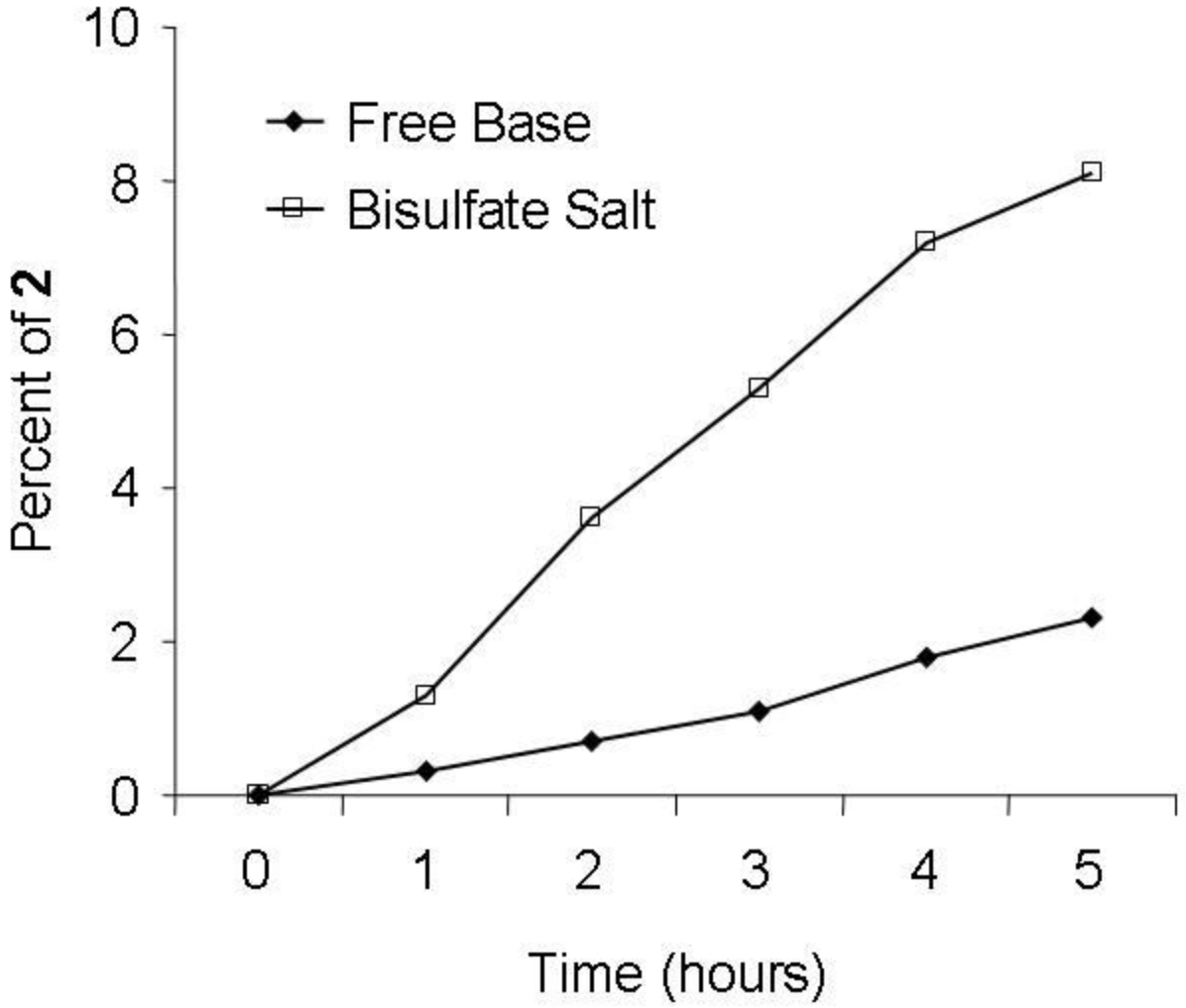

Figure 3

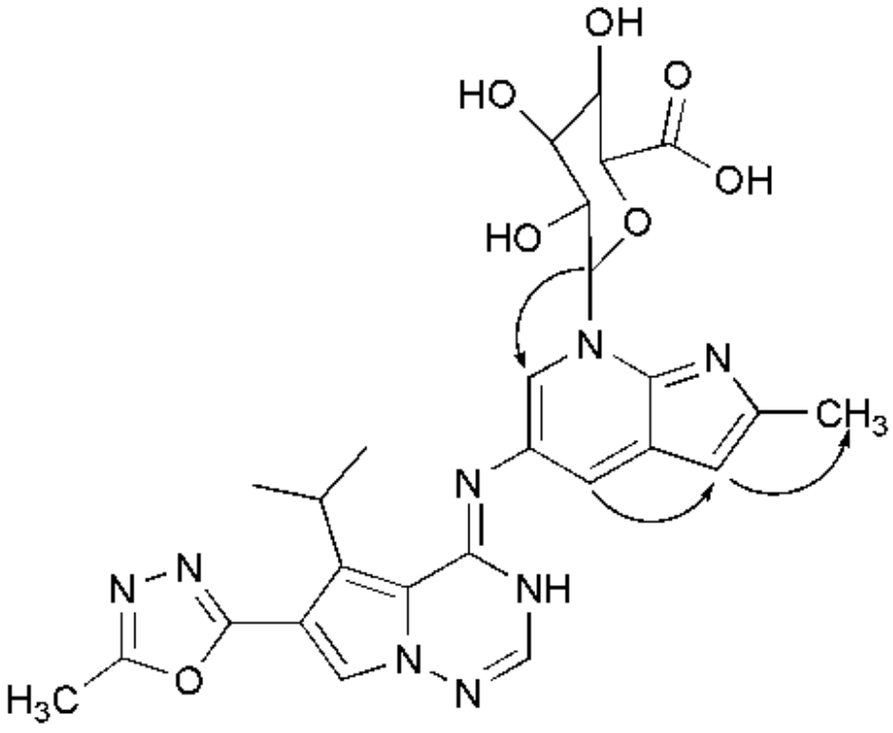
OH
HO
O
OH
HO
O
N
N
CH3
N
N
NH
N
N
O
H3C

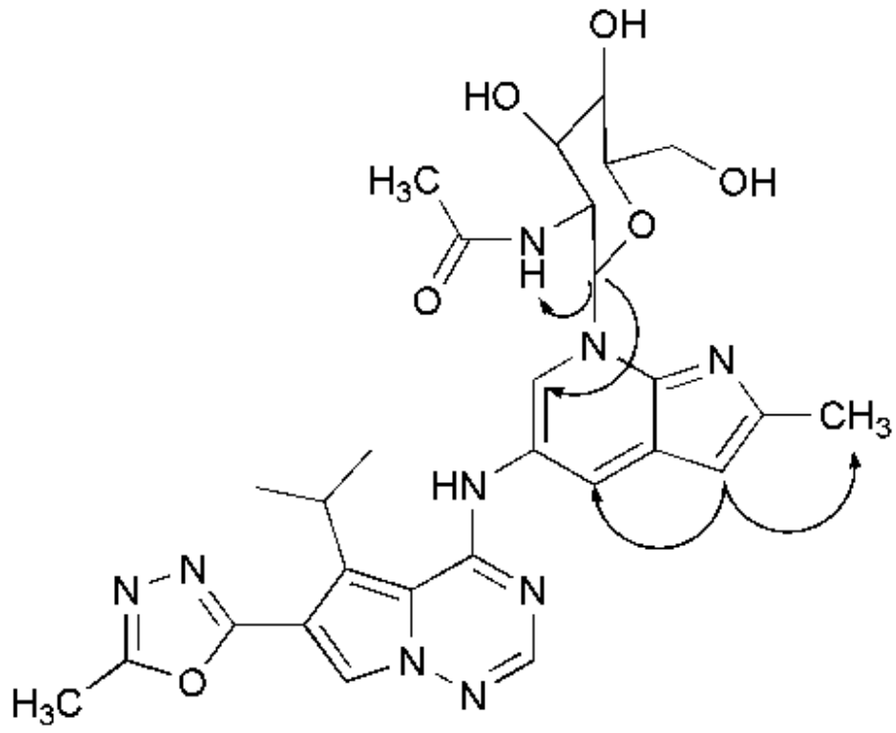
OH
HO
OH
H3C
N
H
O
O
N
N
CH3
HN
N
N
N
N
O
H3C

Fig 4